SCIENCE CHINA
Technological Sciences

Special Topic: Structural Integrity
•Article•

December 2021 Vol.64 No.12: 2608–2617
https://doi.org/10.1007/s11431-020-1902-7

The pitch-catch nonlinear ultrasonic imaging techniques for structural health monitoring

CHENG JingWei[1*], DRINKWATER Bruce W.[2], CHEN XueDong[1], FAN ZhiChao[1], CHEN Wei[1] & WANG Zhe[1]

[1] *National Safety Engineering Technology Research Centre for Pressure Vessels and Pipelines, Hefei General Machinery Research Institute Co. Ltd., Hefei 230031, China;*
[2] *Department of Mechanical Engineering, University of Bristol, Bristol BS8 1TR, United Kingdom*

Received December 30, 2020; accepted July 23, 2021; published online September 18, 2021

Nonlinear ultrasonic imaging techniques in pulse-echo configuration have recently shown their potential to allow the effective separation of nonlinear and linear features in a nonlinear image. In this study, two ultrasonic phased arrays are implemented to produce an image of elastic nonlinearity through the parallel-sequential subtraction of the coherently scattered components in the through-transmission acoustic field at the transmission or subharmonic frequency. In parallel mode, a physical focus at each pixel is achieved by firing the transmitters with a predefined delay law. In sequential mode, each transmitter is fired in sequence and all the receivers are employed to capture the data simultaneously. This full matrix captured data can be post-processed and focused synthetically at the target area. The images of parallel focusing and sequential focusing are expected to be linearly identical and hence any differences remained on the subtracted image can be related to the nonlinearities arising from the defects. Therefore, the imaging metric here is defined as the difference between parallel and sequentially focused amplitudes obtained from forward coherently scattered fields at each target point. Additionally, the negative influences due to the instrumentation nonlinearities are investigated by studying the remaining relative phase and amplitude at undamaged pixels. A compensation method is implemented to suppress these noises, significantly enhancing the selectivity of nonlinear scattering features. The proposed techniques are then implemented to monitor fatigue crack growth in order to explore the capability of these methods as measures of elastic nonlinearity induced by different sizes of small closed cracks. The promising results suggest that nonlinear imaging can be used to monitor crack growth and improve the detectability at early stages.

pitch-catch coherent measurement, nonlinear imaging, fatigue crack monitoring, ultrasonic phased array, nonlinearities decoupling

Citation: Cheng J W, Drinkwater B W, Chen X D, et al. The pitch-catch nonlinear ultrasonic imaging techniques for structural health monitoring. Sci China Tech Sci, 2021, 64: 2608–2617, https://doi.org/10.1007/s11431-020-1902-7

1 Introduction

Nonlinear ultrasonic techniques using phased arrays have recently emerged with the capability to image and quantify fatigue cracks [1,2]. The physically opening and closed state of microcrack gives rise to the nonlinear dynamics with oscillating breathing stiffness and friction damping [3,4]. This non-classical behavior of the microcrack leads to a measurable nonlinear response before the formation of the macroscopic cracks, to which the linear ultrasound is sensitive. The so-called contact acoustic nonlinearity (CAN), known as non-classical nonlinearity can be attributed to a hysteretic behavior [5] or a clapping effect [6,7]. Previous studies investigated the feasibility of second harmonic generation and frequency modulation methods to measure acoustic nonlinearity by using single-element transducers. Despite the

*Corresponding author (email: jingwei.cheng@hotmail.com)

ability to spatially identify fatigue cracks and quantitatively measure their sizes at early stages [8–12], the complex experimental setups and the large measurement errors have resulted in a clear gap between laboratory tests and engineering practice [13–21].

Over recent years, nonlinear ultrasonic imaging techniques in which a single array probe is employed have been demonstrated to deliver immense potential for visualizing partially closed fatigue cracks. These techniques predominantly evaluate the subharmonic components or the fundamental loss from the nonlinearly distorted waves in a pulse-echo configuration. The first developed technique, subharmonic imaging [22] analyzed subharmonics in the measured waves backscattered from open and closed cracks in metallic structure. However, this class of method necessitates suppression of the superposition between fundamental and subharmonic frequency components. Another class of technique selects the fundamental components in coherently backscattered field to quantify elastic nonlinearity at or close to the target point [23,24]. The principle is that a considerable portion of fundamental energy will transfer to some other frequency components and the relative fundamental loss between different transmission modes (e.g., amplitude modulation and parallel-sequential field subtraction) can be measured, whereby the source of elastic nonlinearity is expected to be detected. However, such a technique still necessitates further development to improve the detectability of weak backscatterer as well as suppress interference from linear features. The third class of method measures uniformly distributed energy in the diffuse field including total nonlinear information at each pixel location [25,26]. Whist this technique is seen to provide the high sensitivity to closed cracks by capturing more nonlinear information from the forward scattered waves in the diffuse field, the requirement of measurable signals in the diffuse field has limited its application.

This paper presents a novel form of fundamental and subharmonic frequency component imaging technique in which the forward scattered field is explored by implementing the pitch-catch setup (i.e., through-transmission measurements). This method is manifested to have significant benefits over the approaches mentioned above. Two phased array probes are placed on opposite sides of the component, such that element firing and data capture are realized independently in order to measure the forward scattered nonlinear components of the parallel coherent field and sequential coherent field, respectively. Pitch-catch nonlinear ultrasonic coherent imaging (hereinafter referred to as p-NCI) methods are explored and developed by observing the novel nonlinear phenomena in terms of phase change and amplitude loss primarily at the fundamental or subharmonic frequency. In addition, an approach of the pitch-catch instrumentation nonlinearities compensation is proposed to significantly improve the detectability of microcracks. Promising experimental results are demonstrated for the p-NCI approach and used to quantitatively monitor fatigue crack growth from 20000 fatigue cycles (corresponding to 350 μm long crack). In addition, the effective localization of the crack tip as well as favorable detection sensitivity reliably delivered by this approach facilitates the practical applications to structural health monitoring of critical engineering components.

2 Principle of p-NCI

The fundamental concept of the p-NCI approach employs two alternative imaging modes of an off-the-shelf phased array system, known as parallel focusing and sequential focusing. In parallel focusing the firing of multiple elements with relative delay is implemented and in sequential focusing the separate firing of each element is employed. Their imaging process is as follows. Firstly, a parallel image is produced by physically focusing at each pixel in sequence through a transmitter and a receiver with the equivalent fundamental or subharmonic centre frequency on reception. Secondly, a sequential image is formed in a manner conceptually similar to the total focusing method [27] for the dual array configuration filtered at the fundamental band or subharmonic. Synthetic focusing is then achieved through post-processing of a sequentially captured full matrix. These two focusing methods are expected to be linearly equivalent, inferring that the subharmonic and superharmonic components within the transmission band will be removed after parallel-sequential subtraction. Harmonic generation is by definition [16] an amplitude-dependent process, implying harmonic and subharmonic scattering will be greater for the parallel transmission case due to much larger fundamental energy at the focal point. Consequently, through subtracting these two images from each other, linear geometric features should be removed and only nonlinear scatterers should remain. In this way, the p-NCI method in the subsequent study predominantly examines the characteristics of forward scattered nonlinear response from the microcracks by capturing the parallel focused signals and sequentially transmitted signals in the forward coherent wave field.

For the sequential focusing, we assume that $q_{a,b}(t)$ is the full matrix captured data for each pair of transmitting (a) and receiving (b) elements. Additionally, $p_b(s,t)$ is the time-domain signals received by element b in the parallel case. $\tau_a^{\mathrm{T}}(s)$ is the transmission delay for the a^{th} element and $\tau_b^{\mathrm{R}}(s)$ is the reception delay for the b^{th} element to focus at a pixel location, $s(x,z)$. The Fourier transformed frequency-domain signals in parallel and sequential cases are denoted by $P_b(s,\omega)$ and $Q_{a,b}(\omega)$, respectively. Accordingly, the sequentially

focused signals $Q(s,\omega)$ can be obtained by correspondingly applying transmission delay $\tau_a^{\mathrm{T}}(s)$ and reception delay $\tau_b^{\mathrm{R}}(s)$, which is expressed as

$$Q(s,\omega)=\sum_{b=1}^{N_{\mathrm{R}}}\left(\sum_{a=1}^{N_{\mathrm{T}}}Q_{a,b}(\omega)\mathrm{e}^{\mathrm{i}\omega\tau_a^{\mathrm{T}}(s)}\right)\mathrm{e}^{\mathrm{i}\omega\tau_b^{\mathrm{R}}(s)}. \tag{1}$$

Likewise, the parallel focused signals $P(s,\omega)$ to which the reception delay $\delta_b^{\mathrm{R}}(s)$ in the post-processing is applied may be written as

$$P(s,\omega)=\sum_{b=1}^{N_{\mathrm{R}}}P_b(s,\omega)\mathrm{e}^{\mathrm{i}\omega\tau_b^{\mathrm{R}}(s)}. \tag{2}$$

Subsequently, the filtered parallel signals $\widetilde{P}(s,\omega)$ and filtered sequential signals $\widetilde{Q}(s,\omega)$ are obtained by a filter with considerably narrow band, one third of the nominal center frequency at reception, whereby the nonlinear signals generated from the defects can be selectively measured through minimizing the influence of internally moved energy within the post-processing band [24]. Next, the filtered time-domain signals in the sequential and parallel focusing cases $q(s,t)$ and $p(s,t)$ are calculated through an inverse Fourier transform. Last, the focal time t_f implies time of flight from reference transmitter element to each pixel location and from the pixel location to reference receiver element.

$$t_f=\frac{\sqrt{(x_m-x)^2+z^2}+\sqrt{(x_n-x)^2+z^2}}{c}, \tag{3}$$

where x_m and x_n are the x-axis position of reference transmitter element and reference receiver element for the reception delay law. Consequently, by interpolating the corresponding amplitude at t_f the sequentially focused amplitude intensity A_q at imaging pixel s can be expressed as

$$A_q(s)=\left|q\left(s,t_f\right)\right|. \tag{4}$$

Similarly, the parallel focused amplitude intensity A_p at the imaging pixel s is given by

$$A_p(s)=\left|p\left(s,t_f\right)\right|. \tag{5}$$

Finally, a nonlinear image using metric $\kappa(s)$ can be produced by calculating the subtracted amplitudes between the sequential and parallel focusing as follows:

$$\kappa(s)=\left|q\left(s,t_f\right)-p\left(s,t_f\right)\right|. \tag{6}$$

The prior study [24] has found that the inevitable nonlinearities arising from the instrumentation and experimental setup (e.g., electrical circuit, array elements and gel couplant) can be significantly suppressed in a parallel-sequential subtracted image by nonlinearities decoupling approach using noise compensation factors. However, as a consequence of the measured through-transmission field in this study the reference points of linear features are defined as those pixels within the clean area (i.e., undamaged region containing no linear scatterers). Accordingly, the noise compensations factors of relative phase $\delta_\varphi(\omega)$ and relative amplitude $\delta_A(\omega)$ can be calculated by following the above discussed signal processing steps, thereby computing the corrected sequential amplitude intensity through removal of unwanted nonlinearities, which is as follows:

$$\widehat{Q}(s,\omega)=\frac{\widetilde{Q}(s,\omega)}{\chi_A(\omega)}\mathrm{e}^{-\mathrm{i}\chi_\varphi(\omega)}. \tag{7}$$

Therefore, an improved nonlinear metric $\hat{\kappa}(s)$ by using the corrected time-domain amplitude in sequential case $\hat{q}\left(s,t_f\right)$ can be adjusted to

$$\hat{\kappa}(s)=\left|\hat{q}\left(s,t_f\right)-p\left(s,t_f\right)\right|. \tag{8}$$

3 Experimental procedure

3.1 Experimental setup

The compact tension specimens were fabricated according to the ASTM standard E647-05 and the fatigue test with the equivalent loading conditions used in the previous experiment [26] was conducted thereby relating linear and nonlinear metrics to the size of cracks. In addition, the metallographic preparation was applied to the area around the notch tip prior to the fatigue test. The microstructure in the vicinity of the crack was then identified by a microscope in order to determine the crack size periodically.

Notably, the crack closure is expected to be detectable by the pitch-catch measurement because the complete wave front passing through the crack interface can be collected by another probe located on the opposite side. Additionally, it is worth investigating the nonlinear phenomenon of forward scattered field before the formation of macrocracks. For the experimental setup, a 5 MHz array probe with 64 elements and a pitch of 0.63 mm (manufactured by Imasonic) is implemented as the transmitter in pitch-catch configuration. The dual-sided detection necessitates an additional array probe with centre frequency of 5 or 2.5 MHz for receiving the forward scattered signals at fundamental or subharmonic frequencies (see the details below).

For the fundamental measurement, another identical array probe is used as the receiver for pitch-catch NCI fundamental imaging. The schematic diagram in Figure 1(a) presents the arrangement of the pitch-catch fundamental measurement. Regarding the subharmonic measurement, the nonlinear imaging was achieved by employing a 2.5 MHz array probe with 64 elements and a pitch of 0.5 mm (manufactured by Imasonic) at reception. The schematic diagram in Figure 1(b) describes the layout of the pitch-catch subharmonic measurement. Note that two clamps are employed to keep the probes in good contact with specimens, and a baffle block is used to ensure the consistent alignment of probes.

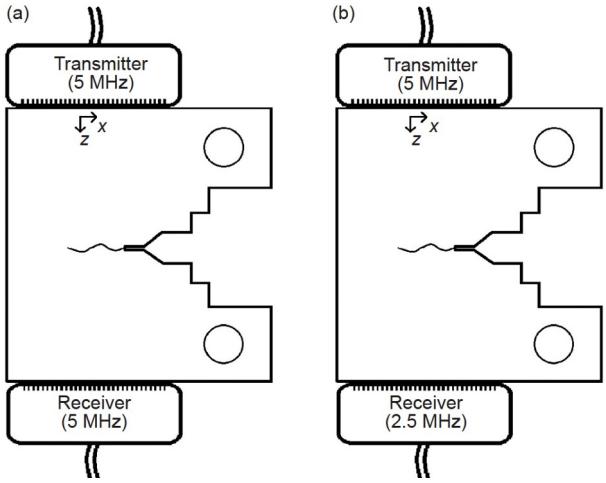

Figure 1 Experimental configuration of (a) pitch-catch fundamental measurement and (b) pitch-catch subharmonic measurement.

3.2 Sequential and parallel forward scattered fields

Example time traces in parallel and sequential cases ($p(s,t)$ and $q(s,t)$) focused at the crack tip in the same CT sample are shown in Figures 2(a) and 3(a). The relative properties of the fundamental and subharmonic wave fields in the frequency domain are displayed in Figures 2(b) and (c) and 3(b) and (c), respectively. It is clear that the parallel and sequential fields focused at the crack tip present significant differences in both phase and amplitude in contrast to those from linear points. The reference linear points here for compensating the instrument nonlinearities are selected to possess an intensity of $A_q(s)$ larger than 0.5. It is worth noting that example focused signals illustrated in Figures 2(a) and 3(a) were used for the frequency analysis.

Notably, the amplitude ratio between sequential and parallel focusing δ_A at the crack tip in the fundamental and subharmonic measurements of p-NCI (as presented in Figures 2(b) and 3(b), respectively) increases by 0.2 and 0.1, respectively compared with that of the pulse-echo measurement results [24]. As a consequence, this delivers remarkable contributions to the same nonlinear metric $\kappa(s)$ as indicated in eq. (6). This observation (i.e., the amplitude of the parallel field is higher than that of the sequential field) as presented in Figures 2(b) and 3(b) shows consistent nonlinear phenomenon with the diffuse energy imaging results [26] in which the remaining fundamental energy of the parallel focusing at the crack tip is much less than that of the sequential one.

On the other hand, the phase difference between the parallel and sequential focusing δ_φ at the crack tip in pitch-catch fundamental and subharmonic measurements at the crack tip reduces by 0.11 and 0.07, respectively relative to that in pulse-echo approach. As a consequence, the phase imaging here is thought to be ineffective for measuring the nonlinearity. This difference in amplitude and phase between

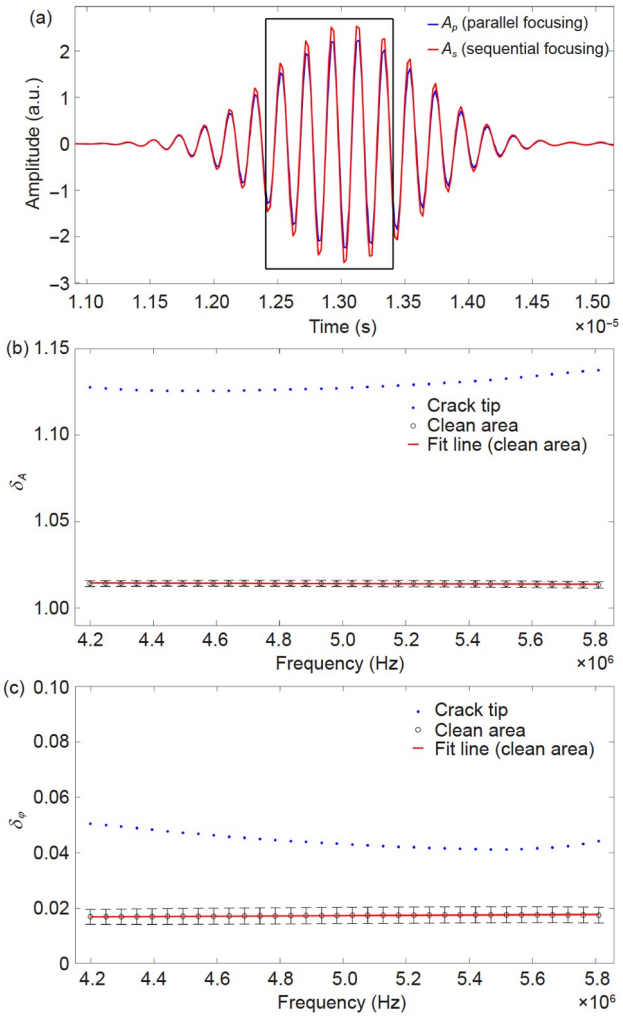

Figure 2 (Color online) Pitch-catch fundamental measurement at 30000 fatigue cycles, (a) time traces focused at the crack tip. The signal used for the frequency analysis is indicated by a black rectangular box. (b) Amplitude ratio δ_A at crack tip and linear points, and (c) relative phase in radians δ_φ versus frequency at the crack tip and linear points. Note that error bars are obtained by calculating standard deviations at selected damage-free area.

backscattered and through-transmission fundamental components induced by closed cracks might be attributed to the nonlinear directivity function at the crack interface. Most importantly, these differences seen in pitch-catch configurations can also be used to image the elastic nonlinearity. The maximum δ_A and δ_φ over the post-processed frequency band at crack tip produced by two p-NCI methods are summarized in Table 1. In addition, it is worth noting their relative change at linear point (clean area) between each method is much smaller compared with that at the crack tip.

4 Imaging process

Figure 4(a) and (b) show the pitch-catch fundamental se-

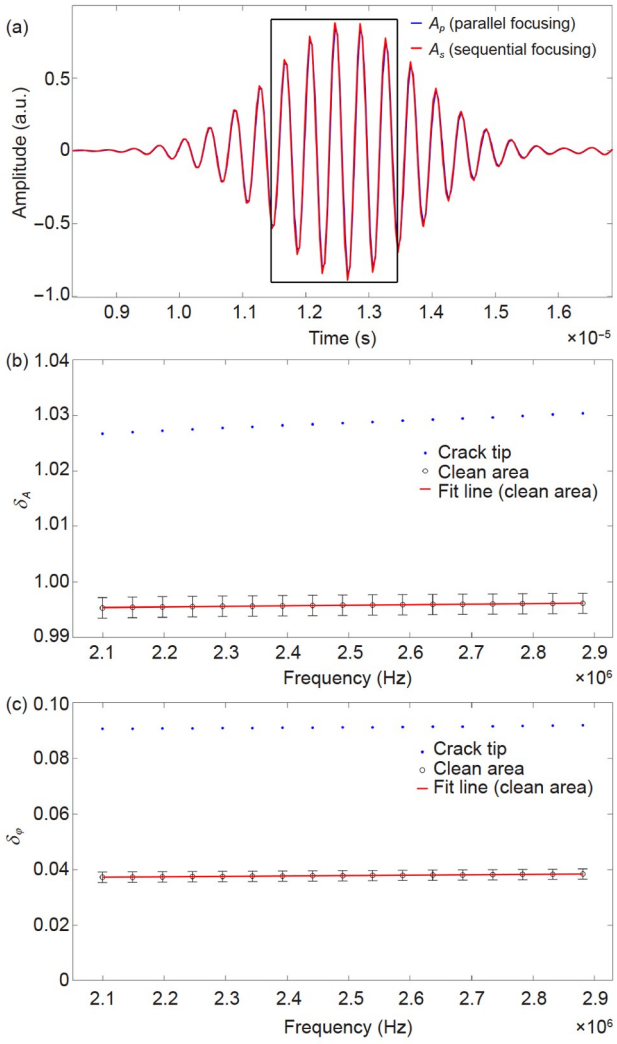

Figure 3 (Color online) Pitch-catch subharmonic measurement at 30000 fatigue cycles, (a) time traces focused at the crack tip. The signal used for the frequency analysis is indicated by a black rectangular box. (b) Amplitude ratio δ_A at crack tip and linear points, and (c) relative phase in radians δ_φ versus frequency at the crack tip and linear points. Note that error bars are obtained by calculating standard deviations at selected damage-free area.

quential and parallel images ($A_q(s)$ and $A_p(s)$) of the area near the notch and the propagating cracks. Note that the absolute amplitude in these linear metrics implies the capability to propagate through the paths between transmitter and receiver. Although these two linearly equivalent images appear to be indistinguishable, the subtracted image (see Figure 4(c)) is capable of selectively identifying the fatigue crack, which is confirmed by the maximum value in the vicinity of the crack tip. Furthermore, an improved nonlinear image with

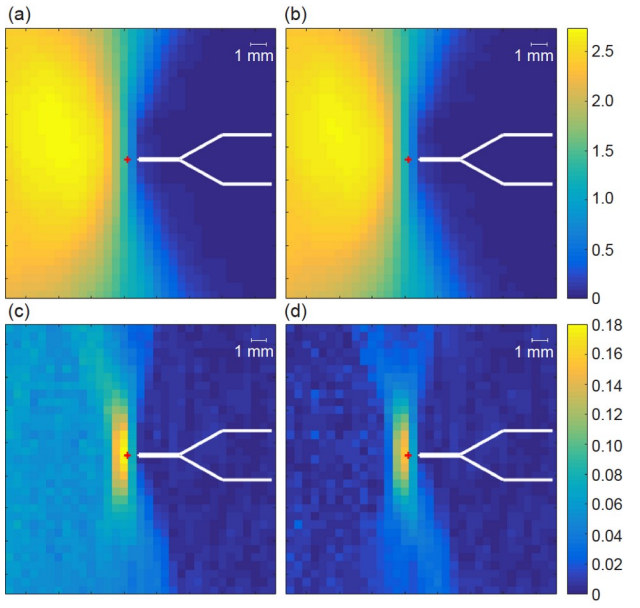

Figure 4 (Color online) Fundamental p-NCI at 30000 loading cycles, (a) sequential image $A_q(s)$ and (b) parallel image $A_p(s)$ in arbitrary units, (c) nonlinear image $\kappa(s)$ and (d) nonlinear image with instrument noise compensation applied $\widehat{\kappa}(s)$. The experimental configuration is as illustrated in Figure 1(a). The crack tip measured by micrography is denoted by a red cross. The white lines indicate the geometries of the electro-discharge machined notch.

the instrumentation compensation process is presented in Figure 4(d), from which it can be observed that the noise level in nonlinear metric reduces roughly from 0.06 to 0.01. Such nonlinear features might be attributed to the principal variation in amplitude, point spread function, and small phase shift.

Likewise, the linear and nonlinear images from the subharmonic measurement are displayed in Figure 5(a)–(d). Their features can be related to those in Figure 4(a)–(d). As a consequence of partial fundamental loss, the nonlinear subharmonic responses indicated by nonlinear images in Figure 5(c) and (d) behave somewhat weaker than the nonlinear fundamental responses measured by those in Figure 4(c) and (d). This is also seen from the smaller δ_φ and δ_A at the crack tip observed in Figure 3(b) and (c). Therefore, the p-NCI of fundamental waves is thought to deliver high selectivity to elastic nonlinearity.

5 Monitoring fatigue crack growth

This study is conducted in order to explore the capability of

Table 1 A summary of amplitude ratio δ_A and relative phase in radians δ_φ at crack tip and linear point (clean area) produced by two p-NCI methods

	δ_A at crack tip	δ_A at clean area	δ_φ at crack tip	δ_φ at clean area
Pitch catch (fundamental measurement)	1.13	1.02	0.05	0.02
Pitch catch (subharmonic measurement)	1.03	1.00	0.09	0.04

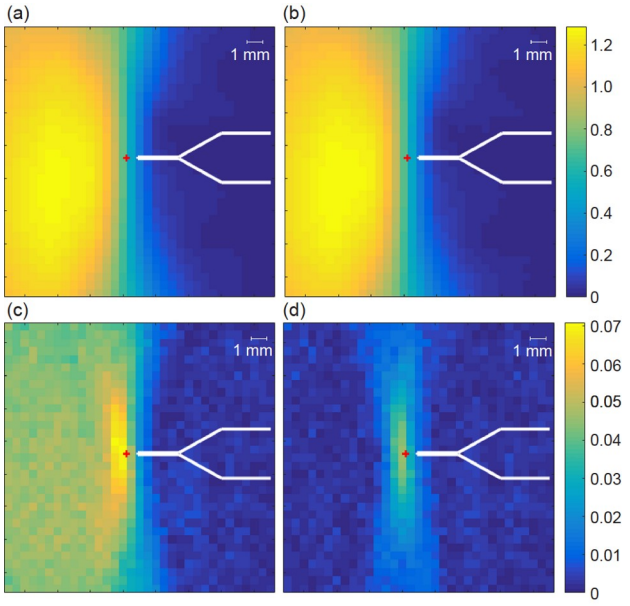

Figure 5 (Color online) Subharmonic p-NCI at 30000 loading cycles, (a) sequential image $A_q(s)$ and (b) parallel image $A_p(s)$ in arbitrary units, (c) nonlinear image $\kappa(s)$ and (d) nonlinear image with instrument noise compensation applied $\hat{\kappa}(s)$. The experimental configuration is as illustrated in Figure 1(a). The crack tip measured by micrography is denoted by a red cross. The white lines indicate the geometries of the electro-discharge machined notch.

forward scattered field as a measure of elastic nonlinearity induced by different sizes of fatigue cracks. In addition, through this study the imaging results may confirm the detection efficacy of each method. The experimental procedures for fundamental p-NCI and subharmonic p-NCI are used in this study. Their experimental configurations are illustrated in Figure 1(a) and (b), respectively. The fundamental p-NCI is expected to detect the crack earlier than the pulse-echo method by capturing through-transmission signals distorted at crack closure. This is because this method does not necessitate the formation of partially open cracks to backscatter the nonlinearly distorted waves. In addition, the subharmonic p-NCI is implemented on this crack monitoring, in order to understand the change in nonlinear subharmonic response with increasing crack size, although its response corresponds to part of the fundamental loss.

5.1 Fundamental measurement

Figure 6(a)–(j) display linear images yielded by linear sequential imaging $A_q(s)$ (indicated in eq. (4)) from 10000 cycles to 100000 cycles. In contrast to the pulse-echo method [24], the pitch-catch sequential image features are more difficult to reveal the actual size of cracks throughout their fatigue life. The change in linear images with increasing cycles predominantly arises from the forward field scattered by the growing cracks. It is seen that the amplitude of through-transmission waves is decreasing with increasing crack length.

However, the pitch-catch nonlinear images $\hat{\kappa}(s)$ obtained from eq. (8) in Figure 7(a)–(j) reveal the presence of microcracks and deliver high selectivity of nonlinear features from 20000 fatigue cycles. The detectability is indicated by nonlinear metric $\hat{\kappa}(s)$ with a value (0.055) higher by a factor of 3 compared with the peak value at the clean area seen at present and earlier stage. Notably, the highest nonlinearity (equal to 0.2205 in $\hat{\kappa}(s)$) throughout its fatigue life is seen at 50000 cycles, which appears slightly earlier than that from pulse-echo measurement [24]. Subsequently, the nonlinearities measured by $\hat{\kappa}(s)$ decrease at an increasing rate with the number of cycles since the crack interface becomes

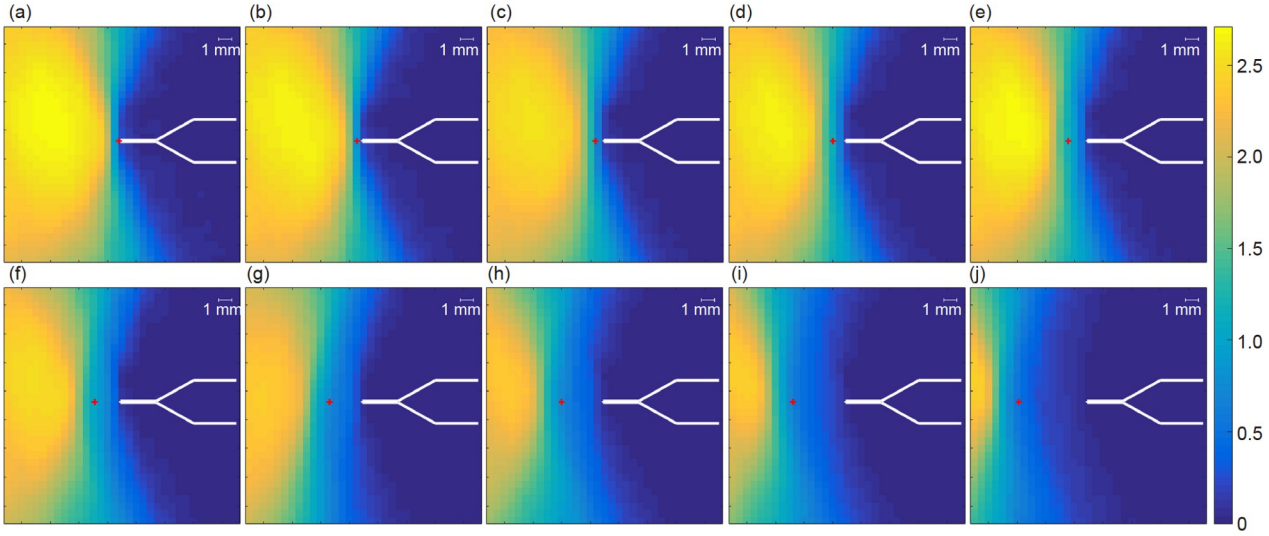

Figure 6 (Color online) Linear sequential images $A_q(s)$ in arbitrary units at (a) 10000 cycles, (b) 20000 cycles, (c) 30000 cycles, (d) 40000 cycles, (e) 50000 cycles, (f) 60000 cycles, (g) 70000 cycles, (h) 80000 cycles, (i) 90000 cycles and (j) 100000 cycles. Figure 1(a) displays the experimental configuration. The crack tip measured by micrography is denoted by a red cross.

increasingly open. It should be noted that the nonlinear responses observed in nonlinear images are principally attributed to the difference in absolute amplitude between sequential and parallel focusing, whilst the phase offset is the dominant nonlinear effect for pulse-echo measurement [24]. Some evidence is provided by similar features seen in the resulting images (as presented in Figure 8(a)–(j)) generated through the subtraction of parallel absolute amplitude $A_p(s)$ from sequential absolute amplitude $A_q(s)$.

5.2 Subharmonic measurement

Figure 9(a)–(j) present similar linear features (as seen in Figure 6(a)–(j)) generated from sequential subharmonic imaging $A_q(s)$ (see eq. (4)) from 10000 to 100000 cycles. As a consequence of the similar features, these linear results might predominantly arise from the linear subharmonic components within transmission bandwidth. Since the region of closed cracks in these linear sequential images does not exhibit any notably high magnitude, the nonlinear subharmonic responses induced by the cracks are thought to be negligible compared with the linear subharmonic components, so that the nonlinearity of cracks cannot be determined by the change in linear images.

However, the subtracted nonlinear images $\hat{\kappa}(s)$ obtained using eq. (8) in Figures 10(a)–(j) reveal comparable non-

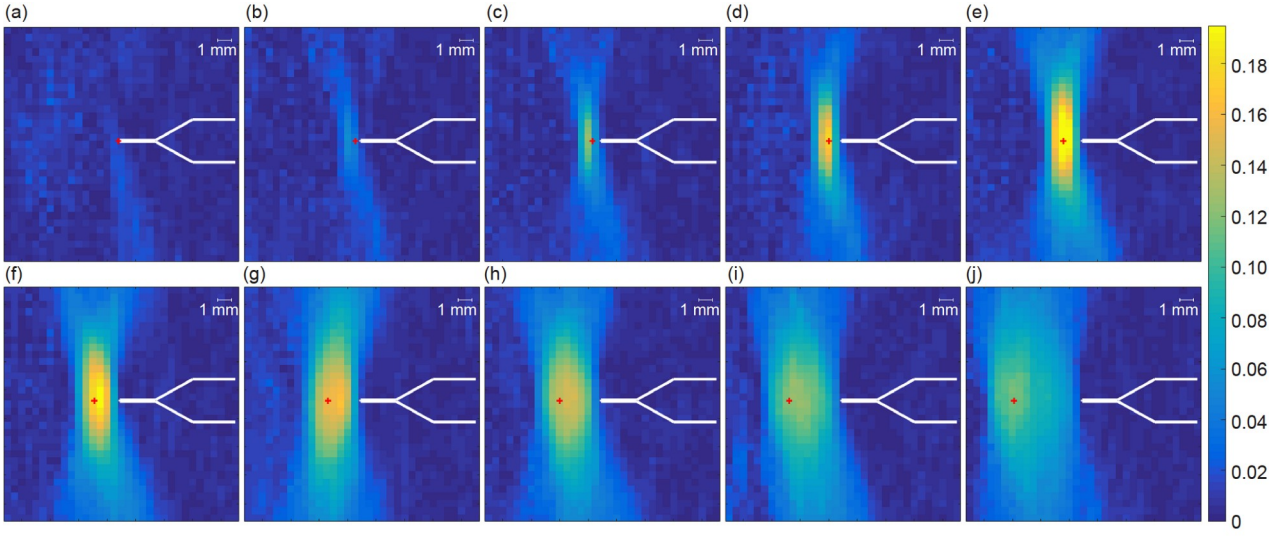

Figure 7 (Color online) Fundamental p-NCI nonlinear images in nonlinear amplitude metric $\hat{\kappa}(s)$ at (a) 10000 cycles, (b) 20000 cycles, (c) 30000 cycles, (d) 40000 cycles, (e) 50000 cycles, (f) 60000 cycles, (g) 70000 cycles, (h) 80000 cycles, (i) 90000 cycles and (j) 100000 cycles. Figure 1(a) displays the experimental configuration. The crack tip measured by micrography is denoted by a red cross.

Figure 8 (Color online) Fundamental p-NCI images obtained by subtracting the absolute values of $A_p(s)$ from $A_q(s)$ at (a) 10000 cycles, (b) 20000 cycles, (c) 30000 cycles, (d) 40000 cycles, (e) 50000 cycles, (f) 60000 cycles, (g) 70000 cycles, (h) 80000 cycles, (i) 90000 cycles and (j) 100000 cycles. Figure 1(a) displays the experimental configuration. The crack tip measured by micrography is denoted by a red cross.

linear features (to those observed in Figure 7) around the cracks and deliver high detectability of crack tip from 30000 cycles in the fatigue life. By comparing with the detectability (earlier detection at 20000 cycles) of fundamental p-NCI, the delay in detecting the crack is primarily due to a small portion of nonlinear responses evaluated in subharmonic p-NCI. Specifically, the earliest detection point at 30000 cycles is confirmed by nonlinear metric $\hat{\kappa}(s)$ with a value (0.043) of the nonlinear metric $\hat{\kappa}(s)$ higher by a factor of 4 relative to the highest background level is seen at present and earlier stage. Notably, the nonlinearities measured by $\hat{\kappa}(s)$ increase to its highest value (equal to 0.1387) at 80000 cycles, which appears much later than those from fundamental p-NCI measurements. Subsequently, the nonlinearities indicated by $\hat{\kappa}(s)$ also decrease at an increasing rate with increasing crack size. Again, the nonlinear responses seen in nonlinear amplitude images $\hat{\kappa}(s)$ primarily arise from the difference in absolute amplitude between sequential and parallel focusing (see Figure 3(b)). Likewise, a solid proof is given by similar features seen in the resulting images (see Figure 11(a)–(j)) generated through the subtraction of parallel absolute amplitude $A_p(s)$ from sequential absolute amplitude $A_q(s)$.

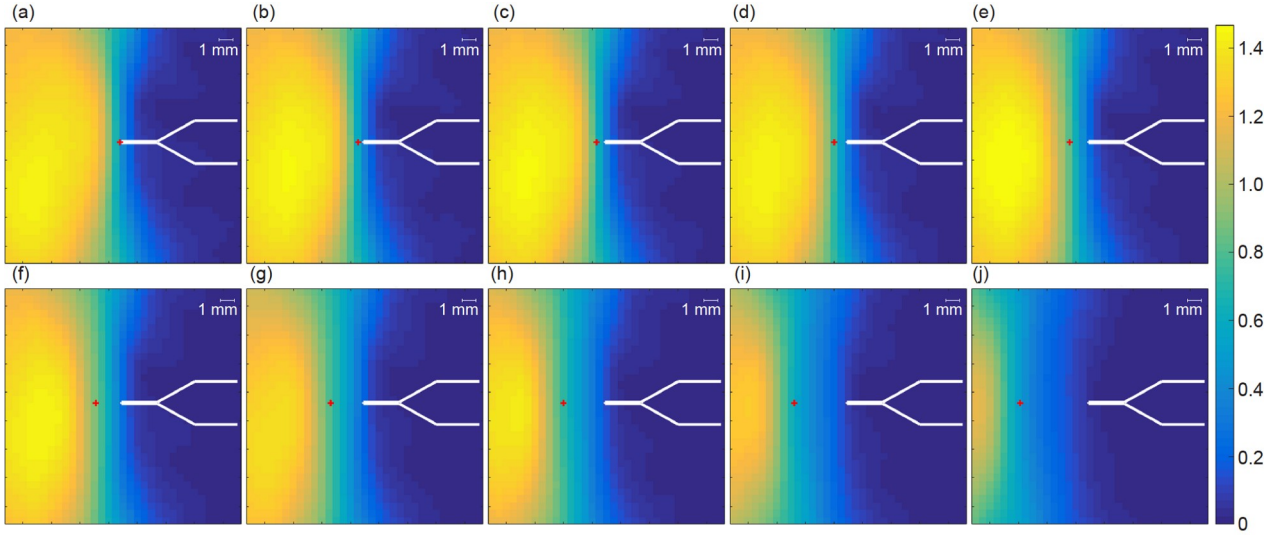

Figure 9 (Color online) Linear sequential images $A_q(s)$ in arbitrary units at (a) 10000 cycles, (b) 20000 cycles, (c) 30000 cycles, (d) 40000 cycles, (e) 50000 cycles, (f) 60000 cycles, (g) 70000 cycles, (h) 80000 cycles, (i) 90000 cycles and (j) 100000 cycles. Figure 1(b) displays the experimental configuration. The crack tip measured by micrography is denoted by a red cross.

Figure 10 (Color online) Subharmonic p-NCI nonlinear images in nonlinear amplitude metric $\hat{\kappa}(s)$ at (a) 10000 cycles, (b) 20000 cycles, (c) 30000 cycles, (d) 40000 cycles, (e) 50000 cycles, (f) 60000 cycles, (g) 70000 cycles, (h) 80000 cycles, (i) 90000 cycles and (j) 100000 cycles. Figure 1(b) displays the experimental configuration. The crack tip measured by micrography is denoted by a red cross.

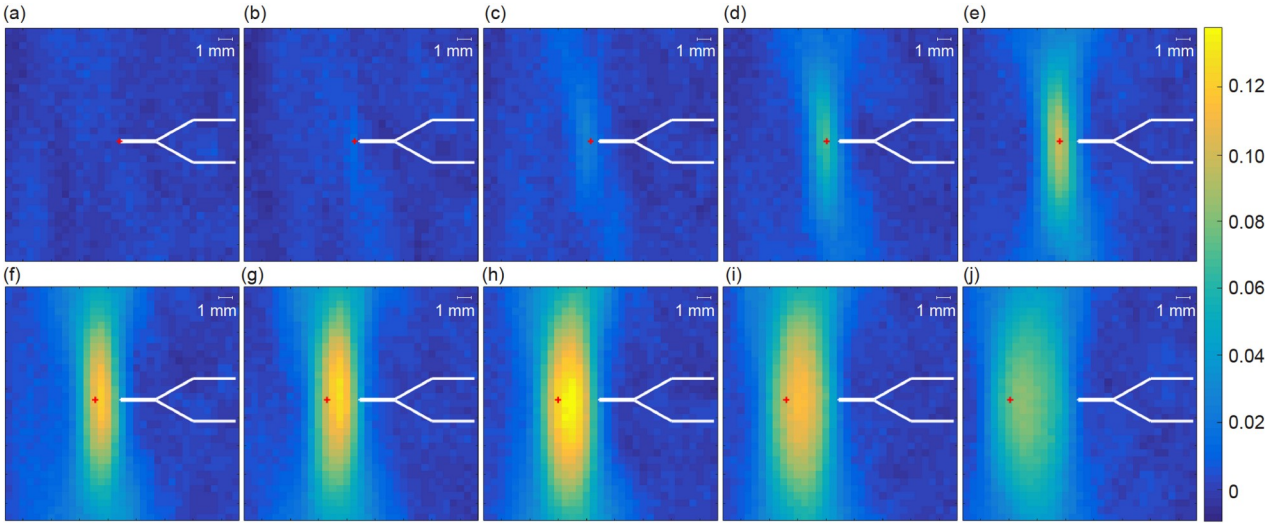

Figure 11 (Color online) Subharmonic p-NCI images obtained by subtracting the absolute values of $A_p(s)$ from $A_q(s)$ at (a) 10000 cycles, (b) 20000 cycles, (c) 30000 cycles, (d) 40000 cycles, (e) 50000 cycles, (f) 60000 cycles, (g) 70000 cycles, (h) 80000 cycles, (i) 90000 cycles and (j) 100000 cycles. Figure 1(b) displays the experimental configuration. The crack tip measured by micrography is denoted by a red cross.

6 Conclusions

A pair of pitch-catch nonlinear ultrasonic coherent imaging techniques (termed as fundamental p-NCI and subharmonic p-NCI) is proposed to selectively detect and size the microcracks based on the measurable differences between parallel and sequentially focused amplitudes obtained from forward coherently scattered fields. Their ability to quantify the microcracks has been demonstrated by monitoring fatigue crack growth in compact tension specimens from a crack length of from 20000 fatigue cycles (corresponding to 350 μm long crack). The sizing of the microcrack was realizable through tracking the maximum nonlinear metric with an accuracy significantly better than 1 mm. In addition, it was manifested that an improved suppression of linear features by applying effective compensation for instrument nonlinearities offered the capability to preferably decouple the nonlinear defect from other geometries (i.e., linear features) particularly in their early fatigue life. Additionally, it is worth noting that both fundamental p-NCI and subharmonic p-NCI are principally dependent on the difference in absolute amplitude between forward scattered fields in parallel and sequential focusing cases. Further, the experimental results suggest that the subharmonic p-NCI approach is less sensitive to the small fatigue cracks in comparison to the fundamental one. This is thought to arise from the amplitudes of the superharmonic components unevaluated by the subharmonic method. The measurement error is found to be within 10% for 5 repeat measurements at different loading cycles. Last but not least, in contrast to pulse-echo coherent field imaging and diffuse field imaging, the proposed p-NCI technique is employed for applications with double-sided access, which is particularly useful for evaluating the nonlinear source containing no reflectors in through-transmission mode. As both techniques show good performance in detection efficacy for fatigue cracks in the early stages of development, these show a promising prospect for structural health monitoring of, for example, pressure equipment and turbines.

This work was supported by the Young Talent Support Program of China Association for Science and Technology (Grant No. [2020] No.87), the Science and Technology Major Project of Anhui Province (Grant No. 201903a05020010), the Key Research and Development Plan of Anhui Province (Grant No. 202004a05020003), the Anhui Provincial Natural Science Foundation (Grant No. 2008085J24), and the Doctoral Science and Technology Foundation of Hefei General Machinery Research Institute (Grant No. 2019010381).

1 Ohara Y, Nakajima H, Haupert S, et al. Imaging of three-dimensional crack open/closed distribution by nonlinear ultrasonic phased array based on fundamental wave amplitude difference. Jpn J Appl Phys, 2020, 59: SKKB01
2 Fierro G P M, Meo M. Non-linear phased array imaging of flaws using a dual and tri frequency modulation technique. Front Built Environ, 2020, 6: 68
3 Liu W, Barkey M E. The effects of breathing behaviour on crack growth of a vibrating beam. Shock Vib, 2018, 2018: 1–12
4 Xie J S, Zi Y Y, Zhang M Q, et al. A novel vibration modeling method for a rotating blade with breathing cracks. Sci China Technol Sci, 2019, 62: 333–348
5 Moussatov A, Gusev V, Castagnède B. Self-induced hysteresis for nonlinear acoustic waves in cracked material. Phys Rev Lett, 2003, 90: 124301
6 Solodov I Y, Korshak B A. Instability, chaos, and "memory" in acoustic-wave-crack interaction. Phys Rev Lett, 2001, 88: 01430
7 Solodov I Y, Krohn N, Busse G. Can: An example of nonclassical acoustic nonlinearity in solids. Ultrasonics, 2002, 40: 621–625
8 Su Z, Zhou C, Hong M, et al. Acousto-ultrasonics-based fatigue damage characterization: Linear versus nonlinear signal features. Mech Syst Signal Processing, 2014, 45: 225–239
9 Lim H J, Song B, Park B, et al. Noncontact fatigue crack visualization

using nonlinear ultrasonic modulation. NDT E Int, 2015, 73: 8–14
10 Fierro G P M, Meo M. Residual fatigue life estimation using a nonlinear ultrasound modulation method. Smart Mater Struct, 2015, 24: 025040
11 Lim H J, Sohn H. Fatigue crack detection using structural nonlinearity reflected on linear ultrasonic features. J Appl Phys, 2015, 118: 244902
12 Amura M, Meo M, Amerini F. Baseline-free estimation of residual fatigue life using a third order acoustic nonlinear parameter. J Acoust Soc Am, 2011, 130: 1829–1837
13 Deng M, Pei J. Assessment of accumulated fatigue damage in solid plates using nonlinear Lamb wave approach. Appl Phys Lett, 2007, 90: 121902
14 Kim J Y, Jacobs L J, Qu J, et al. Experimental characterization of fatigue damage in a nickel-base superalloy using nonlinear ultrasonic waves. J Acoust Soc Am, 2006, 120: 1266–1273
15 Cantrell J H, Yost W T. Nonlinear ultrasonic characterization of fatigue microstructures. Int J Fatigue, 2001, 23: 487–490
16 Solodov I, Wackerl J, Pfleiderer K, et al. Nonlinear self-modulation and subharmonic acoustic spectroscopyfor damage detection and location. Appl Phys Lett, 2004, 84: 5386–5388
17 Croxford A J, Wilcox P D, Drinkwater B W, et al. The use of non-collinear mixing for nonlinear ultrasonic detection of plasticity and fatigue. J Acoust Soc Am, 2009, 126: EL117–EL122
18 Ohara Y, Horinouchi S, Hashimoto M, et al. Nonlinear ultrasonic imaging method for closed cracks using subtraction of responses at different external loads. Ultrasonics, 2010, 51: 661–666
19 Yan Z, Nagy P B. Thermo-optical modulation for improved ultrasonic fatigue crack detection in Ti-6Al-4V. NDT E Int, 2000, 33: 213–223
20 Jiao J P, Drinkwater B W, Neild S A, et al. Low-frequency vibration modulation of guided waves to image nonlinear scatterers for structural health monitoring. Smart Mater Struct, 2009, 18: 065006
21 Ohara Y, Takahashi K, Ino Y, et al. High-selectivity imaging of closed cracks in a coarse-grained stainless steel by nonlinear ultrasonic phased array. NDT E Int, 2017, 91: 139–147
22 Ohara Y, Mihara T, Sasaki R, et al. Imaging of closed cracks using nonlinear response of elastic waves at subharmonic frequency. Appl Phys Lett, 2007, 90: 011902
23 Haupert S, Renaud G, Schumm A. Ultrasonic imaging of nonlinear scatterers buried in a medium. NDT E Int, 2017, 87: 1–6
24 Cheng J, Potter J N, Drinkwater B W. The parallel-sequential field subtraction technique for coherent nonlinear ultrasonic imaging. Smart Mater Struct, 2018, 27: 065002
25 Potter J N, Croxford A J, Wilcox P D. Nonlinear ultrasonic phased array imaging. Phys Rev Lett, 2014, 113: 144301
26 Cheng J, Potter J N, Croxford A J, et al. Monitoring fatigue crack growth using nonlinear ultrasonic phased array imaging. Smart Mater Struct, 2017, 26: 055006
27 Holmes C, Drinkwater B W, Wilcox P D. Post-processing of the full matrix of ultrasonic transmit-receive array data for non-destructive evaluation. NDT E Int, 2005, 38: 701–711